PERGAMON

Journal of Structural Geology 23 (2001) 991–1005

JOURNAL OF STRUCTURAL GEOLOGY

www.elsevier.nl/locate/jstrugeo

Deformation path in high-strain zones, with reference to slip partitioning in transpressional plate-boundary regions

D. Jiang[a,*], S. Lin[b], P.F. Williams[c]

[a]*Laboratory for Structural Geology and Tectonics, Department of Geology, University of Maryland, College Park, MD 20742, USA*
[b]*Department of Earth Sciences, University of Waterloo, Waterloo, ON, Canada N2L 3G1*
[c]*Department of Geology, University of New Brunswick, Fredericton, NB, Canada E3B 5A3*

Received 26 January 1999; accepted 28 August 2000

Abstract

The current status of the kinematics and strain geometry of high-strain zone studies is briefly summarized. A general high-strain zone has a triclinic deformation path, and monoclinic shear zones are special end member cases. Fabrics observed in natural shear zones and theoretical considerations based on continuum mechanics are compatible with this conclusion. Non-steady deformation paths remain difficult to deal with, and may ultimately rely on a realistic mechanical treatment of high-strain zones which may be possible when our knowledge of the mechanical behavior of rocks under natural deformation conditions is improved. An examination of the phenomenon of slip partitioning in transpressional plate boundary regions shows that the bulk deformation path in the forearc area (trench-parallel high-strain zone) is generally triclinic. The Alpine Fault in the South Island of New Zealand provides an example of a currently active triclinic shear zone. The Southern Knee Lake shear zone of Manitoba, Canada, provides an Archean example of a triclinic shear zone.

1. Introduction

Localization of strain into high-strain zones is a common phenomenon on all scales of natural deformation and has been the topic of a large number of studies. In this contribution, we first briefly summarize the current status of the understanding of the kinematics and strain geometry of high-strain zones. Second, after examining the partitioning of the relative plate movement in transpressional plate boundary regions, we suggest that the bulk deformation path in these regions is likely to be triclinic in general. Third, we apply our understanding of slip partitioning and high-strain zone deformation to two natural high-strain zones—the currently active Alpine fault in New Zealand, where both the boundary movement and the internal strain geometry can be independently determined, and an Archean shear zone (Southern Knee Lake shear zone) in a greenstone belt in northern Manitoba, Canada. Both shear zones exhibit strain geometry that cannot be explained by monoclinic shear zone models, but fit the predictions of triclinic high-strain zones (Jiang and Williams, 1998a,b; Lin et al., 1998).

2. Historical overview and current status

2.1. General statement

Modern studies of the geometry and kinematics of ductile shear zones started with the simple shear model proposed by Ramsay and Graham (1970; see also Ramsay, 1980). Ramberg (1975a,b) considered constant-volume steady-state deformation situations as various combinations of pure and simple shear. Sanderson and Marchini (1984) proposed a three-dimensional model where a vertical shear zone has strike-slip and the zone thins (transpression) or thickens (transtension) in response to zone-normal compression or extension. In their model, the strike length and volume are constant so that boundary-normal shortening or extension are compensated completely by vertical stretch. Their model predicts that, for a vertical transpressional shear zone, the maximum principal finite strain axis will be either horizontal or vertical. This point was made more explicitly by Fossen and Tikoff (1993; see also Tikoff and Fossen, 1993) who reformulated Sanderson and Marchini's model following Ramberg (1975a,b), but expressed the flow kinematic quantities, such as the kinematic vorticity number, in terms of finite strain parameters assuming a steady-state deformation history. They show

* Corresponding author. Fax: +1-301-314-9661.
E-mail address: dzjiang@geol.umd.edu (D. Jiang).

0191-8141/01/$ - see front matter
PII: S0191-8141(00)00170-X

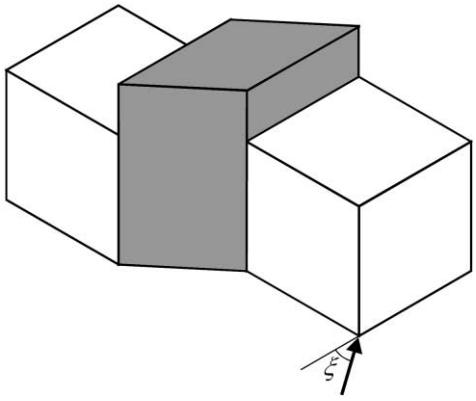

Fig. 1. A simple thinning zone (constant strike length and volume)—Sanderson and Marchini (1984) type transpression zone. For such a zone the value of the angle ξ between the convergence vector and the zone boundary reveals a lot about the kinematics and strain geometry of the zone. When $\xi = 0°$, the zone is a Ramsay and Graham (1970) shear zone; when ξ is greater than 20° the maximum principal strain axis is always vertical; when ξ is less than 20° the maximum principal strain axis starts horizontal but switches to vertical at higher strains. The strain value at which the switching takes place depends on the value of ξ. The smaller the angle ξ, the higher the strain value. See text for details.

that for Sanderson and Marchini type zones when the angle ξ between the convergence vector and the zone boundary (Fig. 1) is less than 20°, at lower strains the maximum principal finite strain axis (λ_1) lies in the horizontal plane and the intermediate strain axis (λ_2) is vertical, whereas at higher strains λ_1 switches with λ_2 to become vertical. The strain value at which the 'switching' takes place depends on the value of ξ. The smaller the angle the larger the strain value (Fossen et al., 1994). When ξ is greater than 20°, λ_1 is always vertical. Jones et al. (1997); Fossen and Tikoff (1998); Tikoff and Fossen (1999) considered the strain geometry of constant volume transpression and transtension zones where change in strike-length during deformation is allowed. These extensions of the Sanderson and Marchini model open more possibilities for structural interpretation. All the above-mentioned models have monoclinic symmetry, and they can be completely characterized by four variables (Jiang and Williams, 1998a,b; Jiang 1999). These models produce monoclinic finite strain geometries with the vorticity-normal section (VNS) being the symmetry plane (Jiang and Williams 1998a; Lin et al., 1998). Using thinning zones [i.e., zones that get 'thinner' as a result of strain (Jiang and Williams, 1998a) as opposed to zones that get 'narrower' (Means, 1995) by their instantaneous boundaries migrating through the rock material] as examples, the strain geometry is summarized and compared with the simple shear zone of Ramsay and Graham (1970) in Fig. 2.

Passchier (1997, 1998) summarizes all monoclinic models that form a subset of the unified model of Jiang and Williams (1998a). However, no monoclinic models can adequately explain the commonly observed phenomenon in many natural subvertical shear zones of lineations that vary between vertical and horizontal (Hudleston et al., 1988; Lin, 1992; Robin and Cruden, 1994; Goodwin and Williams, 1996; Lin et al., 1998; this study). Robin and Cruden (1994) considered a vertical transpressional shear zone where the boundary-normal convergence is accommodated by vertical extrusion and the boundary-parallel velocity component is taken up by homogeneous simple shear across the zone. The finite strain geometry of their model has been investigated by Dutton (1997). Dutton (1997) also developed the steady-state transpression concept, where the instantaneous zone boundaries migrate through material (widening in the sense of Means, 1995) so that the zone maintains a constant thickness despite being thinned (Jiang and Williams, 1998a) in response to strain. So far we are not convinced that the strain geometry predicted by this model resembles any field data for lineations and foliations. In our opinion, the assumption of this model that the boundary-parallel and boundary-normal components of velocity are accommodated in the same volume of rock is unrealistic. Natural shear zones generally suggest localization of the simple shear component (see further discussion in Lin et al., 1998, 1999), as do theoretical models (England et al., 1985; England and Jackson, 1989) and observation of current plate-boundary deformation (Gordon, 1995).

Lin et al. (1998) considered constant volume and constant strike length thinning- and thickening-zone deformations. Allowing the simple shear component to have a dip-slip component, their model produces generally triclinic deformation paths with the Sanderson and Marchini (1984) model being an end member. The model is further generalized by Jiang and Williams (1998a), who take into consideration volume change as well as biaxial stretching of the zone boundaries. Therefore the model of Jiang and Williams (1998a) unifies all existing shear zone models. This general framework has been used to examine evolution of structures such as folds in shear zones (Jiang and Williams, 1999a).

2.2. The problem of non-steady-state deformation path

All kinematic models are based on the assumption of a steady state progressive deformation. A non-steady deformation history, common in nature (e.g., Lister and Williams 1983; Jiang 1994a,b; Jiang and White 1995), remains a dilemma. If the actual deformation path can be determined, it is potentially possible to approach non-steady histories numerically (Eqs. (7)–(14); McKenzie, 1979; Eqs. (16)–(18); Jiang and Williams, 1998a). The all-important problem, however, is how to constrain a natural deformation path. Fossen and Tikoff (1997) assume that a shear zone achieves a prescribed 'offset' with a non-steady 'minimum strain path'. However, a minimum strain path depends on the choice of 'displacement'; it is not unique. Further, an energetic process such as deformation is unlikely to follow a path that is determined purely on the basis of kinematics

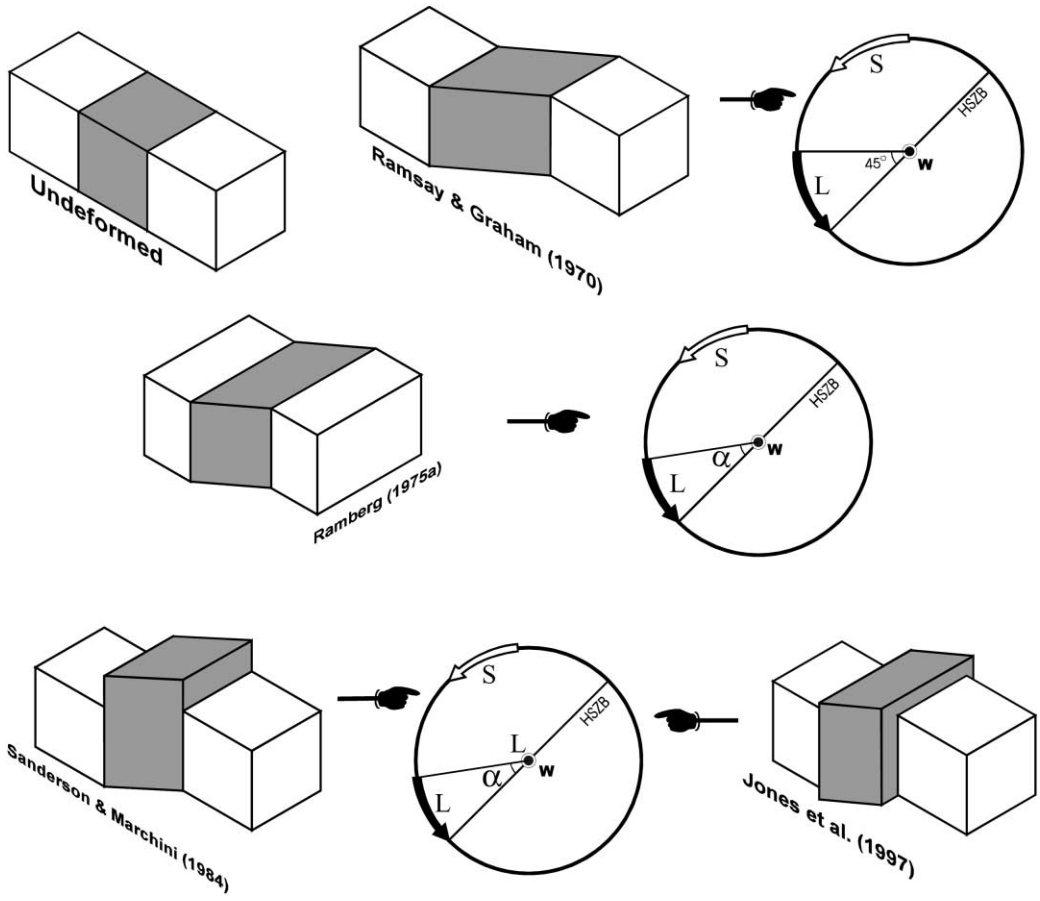

Fig. 2. Strain geometry of monoclinic thinning zones compared with that of Ramsay and Graham's (1970) simple shear zone. The minimum finite strain (λ_3) axes (poles to 'foliations', S) plot on the vorticity-normal sections (VNS, shown horizontal); the maximum finite strain (λ_1) axes ('lineations', L) plot either on the VNS or are parallel to the vorticity vector (**W**). For the Ramsay and Graham (1970) simple shear zone, the λ_1-axis starts at 45° to the high-strain zone boundary (HSZB) and rotates progressively towards parallelism with the boundary as strain increases. For non-simple shear paths, the λ_1-axis may be parallel to the vorticity vector (see text for details) or may plot on the VNS. In the latter case, the λ_1-axis starts at an angle $\alpha(=\cos^{-1}W_k^s)$ with the zone boundary, where W_k^s is the sectional kinematic vorticity on the VNS (Jiang and Williams, 1998a); as strain increases it rotates progressively towards the HSZB and may switch with the λ_2-axis and become parallel to the vorticity vector (see text for details).

(Jiang, 1998). Therefore a non-steady-state path obtained through the minimum strain approach adds no more realism than a steady-state path.

The ultimate approach towards a natural deformation path is, in our opinion, that of a forward modeling (Jiang and Williams, 1999b) based on a sound understanding of the mechanical behavior of rocks (Fletcher and Pollard, 1999). The kinematic path of a deformation is embedded in its mechanical solutions, and as pointed out by Fletcher and Pollard (1999), a complete mechanical approach will allow more fundamental questions to be asked. However, we envisage the following difficulties with a complete mechanical treatment of many natural deformations including high-strain zones, at present. First, the constitutive equations for rocks under different deformation conditions are poorly known. Although a large number of laboratory experiments show that, at steady state, the rheology of a rock may approximate a power law fluid (e.g., Carter and Tsenn, 1987; Tsenn and Carter, 1987; Kohlstedt et al., 1995), transient flow behaviors (flow stress variation as a result of strain increase and/or strain rate variations) commonly expected in rock deformation (Carter and Kirby, 1978; Poirier 1980; Hobbs and Ord 1988) are particularly poorly understood. The realism of a deformation path based on a complete mechanical modeling is, after all, dependent on the appropriateness of our selected constitutive equations. Second, to treat a natural deformation system such as a high-strain zone as a boundary value and/or initial value problem is itself problematic. The boundary (and initial) values are poorly defined. The boundaries commonly migrate through the material, and physical conditions acting via the boundaries are time-dependent. This implies that the boundary properties and the boundary and initial values are all to be expressed as functions of time. We still know too little to describe them realistically. Third, natural deformation is coupled with other geological processes such as metamorphism and magmatism (e.g., Brown and Solar, 1998a,b), which further complicates the problem. Because of these various difficulties, we think that the kinematic approach, of dealing with deformation without regard for

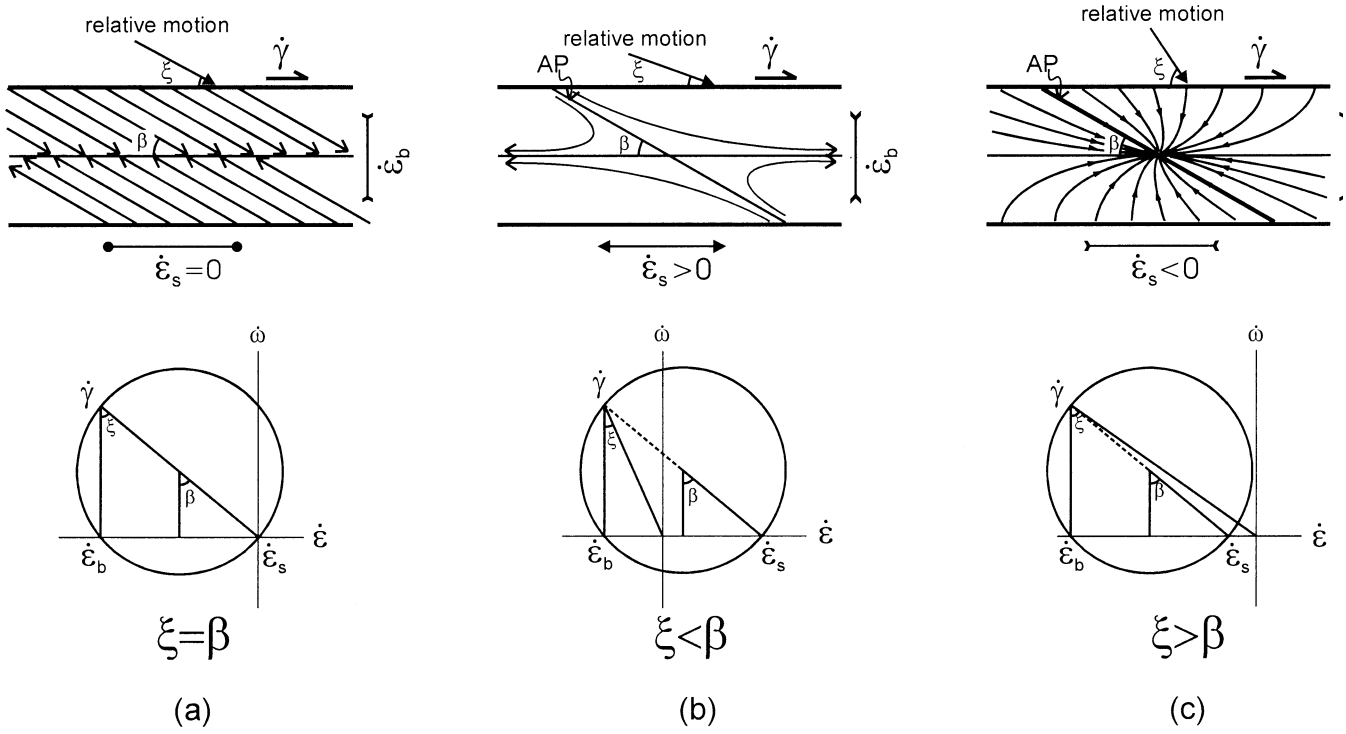

Fig. 3. The relationship between the relative convergence vector and the oblique flow apophysis (AP) for monoclinic transpression, showing that these directions are *not* parallel except when the strike length is constant during deformation. Top row: Simplified geometrical relationship between relative motion, oblique flow apophysis (AP) and particle paths (curved arrows) for: (a) strike-length constant, (b) strike-length increasing, and (c) strike-length decreasing situations. $\dot{\epsilon}_s$, $\dot{\epsilon}_b$ and $\dot{\gamma}$ stand for rate of strain along strike, rate of strain across the zone and the shear strain rate parallel to the zone, respectively. The relative motion direction ξ is related to the strain rates by $\xi = \tan^{-1}|\dot{\epsilon}_b/\dot{\gamma}|$ (Jiang and White 1995) whereas the orientation of AP, β, is related to the sectional kinematic vorticity, W_k^s, by $\beta = \cos^{-1}W_k^s$ (cf. Bobyarchick 1986). Bottom row: Mohr circles showing the difference between ξ and β.

its causes, is still the most effective approach for most natural deformations. The very fact that similar structural patterns occur repetitively in nature may indicate that only limited kinematic paths are mechanically feasible, and improved understanding of such paths will bring us closer to a complete understanding of the mechanical processes.

2.3. Boundary movement and flow properties in high-strain zones

In a general high-strain zone, there are no simple relationships between the relative movement vectors between the two boundaries, the instantaneous stretching axes, the flow apophyses, and the principal stress axes or the finite strain axes. If the material is isotropic and remains so during deformation, then the principal stress axes will coincide with the instantaneous stretching axes. For the Sanderson and Marchini-type transpression zone (i.e., monoclinic, constant volume and constant strike length), Fossen et al. (1994) point out that the relative movement vector between the two boundaries is parallel to the oblique flow apophyses ($\xi = \beta$, Fig. 3a). This statement has been incorrectly extended to more general situations by Fossen and Tikoff (1998) and Dewey et al. (1998). We show in Fig. 3 that only for strict Sanderson and Marchini type zones, does $\xi = \beta$ (Fig. 3a). For strike-length-increasing monoclinic zones, $\xi < \beta$ (Fig. 3b) and for strike-length-decreasing monoclinic zones, $\xi > \beta$ (Fig. 3c). There are no simple relationships for triclinic zones.

2.4. Deformation path and stress field

We have concluded, based on natural observation and theoretical modeling, that triclinic deformation paths are common and monoclinic deformation paths are special cases (Jiang and Williams 1998a,b; Lin et al. 1998, 1999). The fact that mylonites in shear zones commonly exhibit monoclinic fabric does not argue against this conclusion, because one important result of our theoretical modeling is that when the ratio of the simple shear component to the pure shear component ($\dot{\gamma}/\dot{\epsilon}_b$) is high ($>10$), the resulting finite strain geometry *appears* monoclinic within the resolution of observation (Jiang and Williams, 1998a; Lin et al. 1998). Natural deformation has a tendency to localize simple shear (Lin et al. 1998, 1999) and mylonite zones therefore generally represent concentration of simple shear.

Passchier (1998) argues that the stress field associated with a ductile shear zone may favor a monoclinic deformation path within the zone. We assert that stress field has no control on deformation path; for a given material the same stress is compatible with different deformation paths.

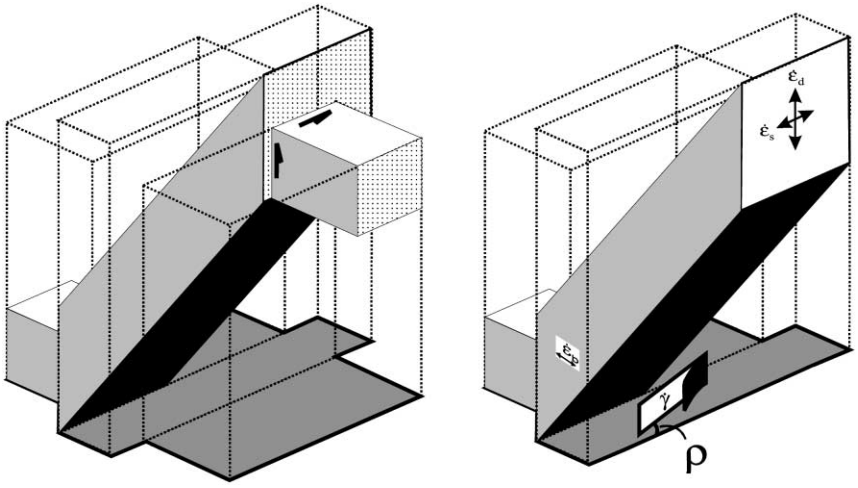

Fig. 4. A homogeneous domain in a general high-strain zone. Five independent parameters are required to completely characterize the rate of deformation. They are: the rate of stretch parallel to the strike $\dot{\epsilon}_s$, the rate of stretch parallel to the dip $\dot{\epsilon}_d$, the thinning rate normal to the zone boundary $\dot{\epsilon}_b$, the shear strain rate parallel to the zone boundary $\dot{\gamma}$, and the angle, ρ, between the shear direction and the strike of the zone.

A popular line of thinking among structural geologists, inherited perhaps from mechanics of elastic materials, is that stress is commonly prescribed, while kinematic variables such as strain are to be calculated from stress. In considering flow problems, it is far more instructive to regard stress as a material response to deformation where, unlike the linear elasticity theory, time (history) becomes an important variable. In a flowing material, the state of stress at a point is directly related to the instantaneous stretching (described by the stretching tensor) only (e.g., Spencer, 1980, p. 105), while the complete characteristics of the flow at a point is defined by both vorticity and stretching. Since the deformation path followed by a material element is the evolution of the characteristics of flow of that material element, it follows readily that the same stress field is theoretically compatible with an infinite number of deformation paths.

The vorticity history that a material element experiences changes the constitutive property of the material, thereby influencing the stress indirectly. The constitutive equation of the rock generally varies during deformation as a result of fabric development. The latter is intimately related to the instantaneous value and the history of the non-coaxiality, which are in turn governed by, amongst other parameters, the instantaneous value and the history of vorticity, respectively (Astarita 1979; Means et al. 1980).

2.5. Finite strain geometry of general high-strain zones

Five independent parameters are required to characterize the rate of deformation of a general high-strain zone (Jiang and Williams, 1998a): the two rates of strain describing the biaxial stretching of the boundaries, $\dot{\epsilon}_a$ and $\dot{\epsilon}_c$ (by definition $\dot{\epsilon}_a \leq \dot{\epsilon}_c$), the rate of strain normal to the zone boundary $\dot{\epsilon}_b$, the shear strain rate $\dot{\gamma}$, and the angle ϑ between shear direction and $\dot{\epsilon}_a$. In this paper for easy reference, we use the strike line of the high-strain zone as a reference orientation by assuming that the rotation of the strike line is negligible during deformation, a reasonable assumption for most large-scale subvertical high-strain zones. In this case, the biaxial stretching of the zone boundaries is described by the rate of strain parallel to the strike of the

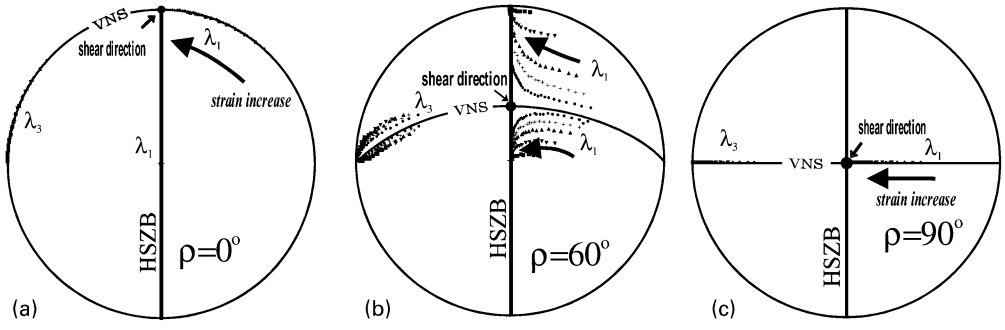

Fig. 5. Equal-area lower-hemisphere projection showing variation and evolution, with progressive deformation, of the maximum (λ_1) and minimum (λ_3) principal finite strain axes for three thinning zone situations ($\rho = 0°$, 90° monoclinic and $\rho = 60°$ triclinic) modified from Jiang and Williams (1998a). Solid square, solid triangle apex down, solid triangle apex up, cross and solid circle stand for $\Theta = 45$, 65, 75, 80 and 85°, respectively. VNS = vorticity-normal section. HSZB = high-strain zone boundary.

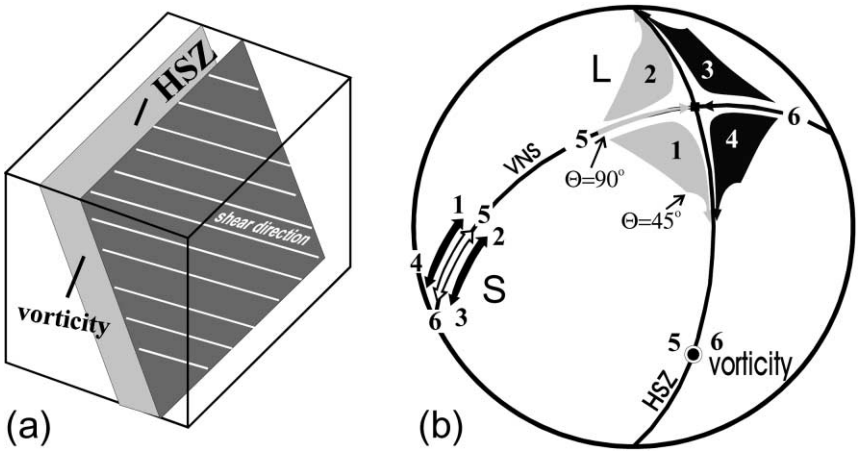

Fig. 6. Schematic diagrams summarizing the theoretical finite strain geometry for various deformation paths. (a) Block diagram of an inclined (so that terms such as reverse and normal can be used) high-strain zone with oblique shear. (b) The resulting finite strain geometry for different cases. S represents λ_3-axes or poles to 'foliations', L represents λ_1-axes or 'lineations'. Arrows point in the direction of increasing strain. See text for details.

zone, $\dot{\epsilon}_s$, and the rate of strain parallel to the dip of the boundaries, $\dot{\epsilon}_d$. The angle between the shear direction and the strike line is denoted by ρ (Fig. 4). $\dot{\epsilon}_s$, $\dot{\epsilon}_d$ and ρ correspond to $\dot{\epsilon}_a$, $\dot{\epsilon}_c$, and ϑ readily. If $\dot{\epsilon}_s \leq \dot{\epsilon}_d$ (dip-lengthening dominant), then $\dot{\epsilon}_s = \dot{\epsilon}_a$, $.\dot{\epsilon}_d = \dot{\epsilon}_c$, and $\rho = \varphi$, and if $\dot{\epsilon}_s > \dot{\epsilon}_d$ (strike-lengthening dominant), then $\dot{\epsilon}_s = \dot{\epsilon}_c$, $\dot{\epsilon}_d = \dot{\epsilon}_a$, and $\rho = 90° - \varphi$.

The kinematics and finite strain geometry of such a general high-strain zone are presented in Jiang and Williams (1998a). A summary is presented here using the above defined $\dot{\epsilon}_s$, $\dot{\epsilon}_d$, and ρ. The deformation paths are triclinic except when $\rho = 0°$ (Fig. 5a), $\rho = 90°$ (Fig. 5c) or $\dot{\epsilon}_s = \dot{\epsilon}_d$. Generally, deformation paths are triclinic and the finite strain geometry for the case of $\rho = 60°$ is shown in Fig. 5b. Different loci of the λ_1- and λ_3-axes are for different ratios of the simple- to the pure-shear components, which are related to the angle Θ between the convergence vector and the zone-boundary normal by $\Theta = \tan^{-1}(|\dot{\gamma}/\dot{\epsilon}_b|)$ (Jiang and Williams, 1998a). Fig. 6 represents the finite strain geometry spatially (Fig. 6a) and on an equal-area net (Fig. 6b). In order to make use of the terms normal, reverse etc., the high-strain zone is inclined. Cases 5 and 6 are monoclinic and both the lineations and poles to foliations plot on the VNS. All other cases are triclinic. Cases 3, 4 and 6 have a normal component of displacement and the lineations plot on the shallower side of the great circle representing the high-strain zone boundary (HSZ); cases 1, 2 and 5 have a reverse component of displacement and the lineations plot on the steeper side of the HSZ great circle. In cases 1 and 4, the dip-lengthening is dominant over strike-lengthening

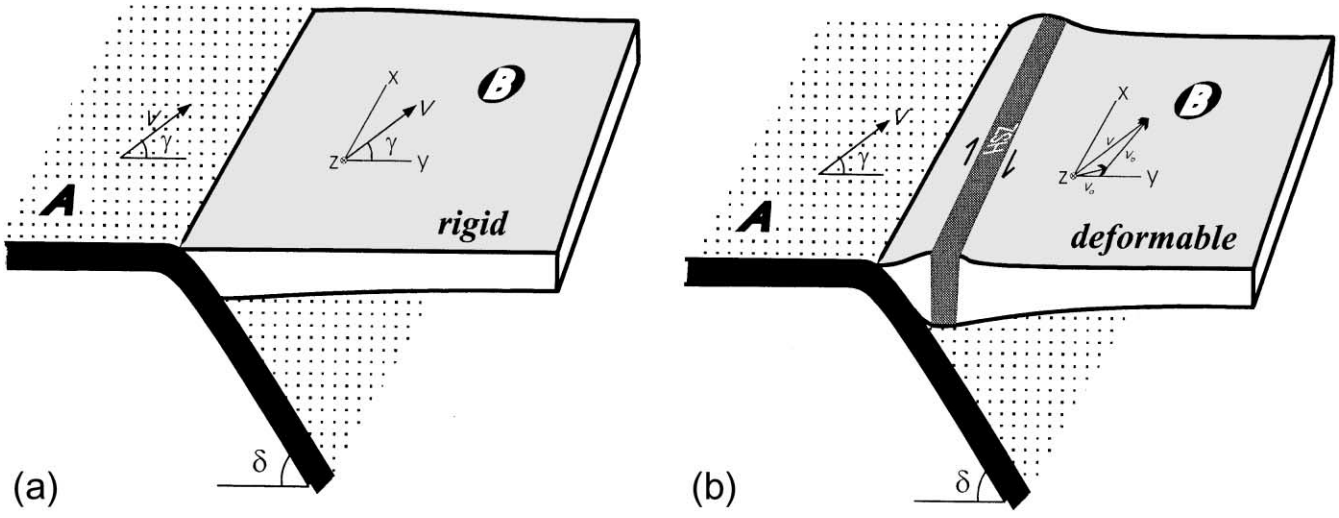

Fig. 7. Geometry and slip partitioning in a transpressional plate boundary. The reference frame is fixed to plate B. (a) When the plates are rigid, the net slip **v** is completely accommodated by interplate slip $\mathbf{v}_a$. (b) When the plates are deformable, the net slip is partitioned into a subduction slip plus a component $\mathbf{v}_b$ taken up by upper plate (trench-parallel high-strain zone) deformation. The angle between net slip and trench normal (γ) is called obliquity of convergence. HSZ stands for high-strain zone. See text for details.

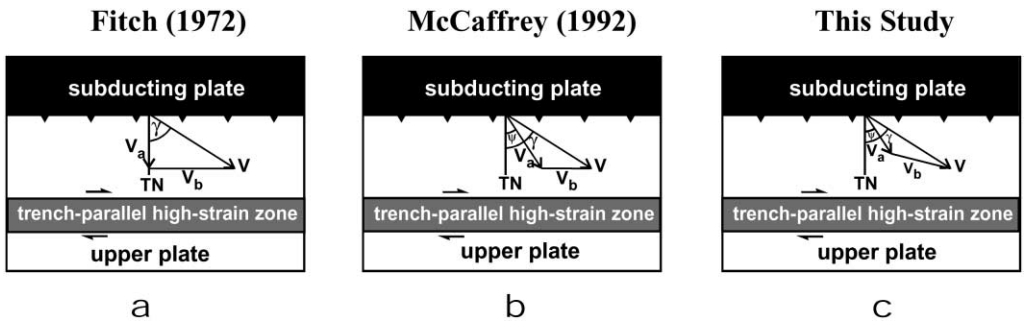

Fig. 8. Models proposed for slip partitioning. See text for further explanation.

($\dot{\epsilon}_d > \dot{\epsilon}_s$), causing the lineations to converge towards the dip line. In cases 2 and 3, strike-lengthening is dominant ($\dot{\epsilon}_s > \dot{\epsilon}_d$) and the lineations converge towards horizontal. For monoclinic cases (5 and 6), the lineations either plot on the VNS and converge towards the shear direction or they are parallel to the vorticity vector.

3. Slip partitioning and bulk deformation path in transpressional plate boundary regions

3.1. Slip partitioning

Most convergent plate boundaries are transpressional in the sense of Harland (1971), with the relative plate velocity oblique to the plate boundaries (Fig. 7, e.g. Fitch, 1972; Beck, 1983; DeMets et al., 1990; McCaffrey, 1992; 1993, 1994, 1996; Liu et al. 1995; Kao et al., 1998). It is the interaction between two plates across the trench that determines plate boundary region deformation. We use a reference frame fixed to one plate (Plate B, Fig. 7) to describe this interaction. The three coordinate axes are: *x*-axis parallel to the trench, *y*-axis horizontal and parallel to the trench-normal, and *z*-axis vertical and pointing down (Fig. 7). The interaction across the trench is described by the net slip, **v**, in Fig. 7. It is easy to see that **v** is the same as the relative velocity between the two plates, if the subducting plate (plate A) has zero roll-back component. Otherwise, **v** is equal to the relative velocity between the two plates subtracting the roll-back component. The angle γ between **v** and the trench-normal (*y*-axis) is called the obliquity of subduction (McCaffrey 1992). Dewey's (1980) three types of arcs, namely extensional, neutral, and compressional, correspond to situations of $\mathbf{v}\cos\gamma$ being negative, zero and positive, respectively. When $\mathbf{v}\cos\gamma$ is negative, the arc is undergoing transtension. We consider neutral to compressional situations only in this paper.

If the two plates (A and B in Fig. 7) are rigid, the net slip is taken up completely by interplate slip, $\mathbf{v}_a$, on the subduction zone, and $\mathbf{v} = \mathbf{v}_a$. Where the plates are deformable, the net slip will be taken up by two mechanisms: the interplate slip $\mathbf{v}_a$ and the upper plate deformation that accommodates a component $\mathbf{v}_b$ (Fig. 7b). This phenomenon is called slip partitioning and can be expressed by the following relationship:

$$\mathbf{v} = \mathbf{v}_a + \mathbf{v}_b. \quad (1)$$

Deformation within the subducting plate is also possible, but this deformation will not affect the following analysis of the relationship between slip partitioning and the upper plate forearc deformation.

Fitch (1972) proposed a model for slip obliquity partitioning (what Fitch called decoupling) in which the net slip either remains unpartitioned (i.e., **v** parallel to $\mathbf{v}_a$), or is completely partitioned into a pure dip slip (i.e., $\mathbf{v}_a$ parallel to trench-normal) accommodated by inter-plate slip in the subduction zone plus a pure strike-slip accommodated by transcurrent shearing within the trench-parallel high-strain zone in the arc (Fig. 8a). Fitch's model was adopted by later authors including Walcott (1978), McKenzie and Jackson (1983), Beck (1983, 1986), Jarrard (1986), Mount and Suppe (1987), Abers and McCaffrey (1988) and Molnar (1988, 1992). Many authors, including Micheal (1990) and Molnar (1992), sought physical explanations for such complete partitioning. However, it was later realized that such complete partitioning is a special, rather than a general, case. Even for the best-known example of Sumatra where such *complete* partitioning is thought to be approached, it is not really complete. According to Molnar (1992), in Sumatra the net slip (**v**) is oriented at about 45° to the strike of the subduction zone, and subduction slip ($\mathbf{v}_a$) is not pure dip-slip but is oriented at about 20° to the trench normal (Fitch, 1972; McCaffrey, 1991). McCaffrey (1992) shows that in many oceanic transpressional subduction zones, subduction slip vectors are neither normal to the trench nor parallel to the net slip. This leads to a more general partitioning scheme (McCaffrey, 1992), shown in Fig. 8b, where γ is the obliquity of net slip and ψ is the subduction obliquity—the angle between $\mathbf{v}_a$ and the trench normal (TN). Cases where $\psi = \gamma$ (no partitioning) or $\psi = 0$ (complete partitioning) are certainly possible, but generally, $0 < \psi < \gamma$, suggesting incomplete obliquity partitioning.

Liu et al. (1995) defined a parameter κ to measure the degree of obliquity partitioning as follows:

$$\kappa = 1 - \psi/\gamma. \quad (2)$$

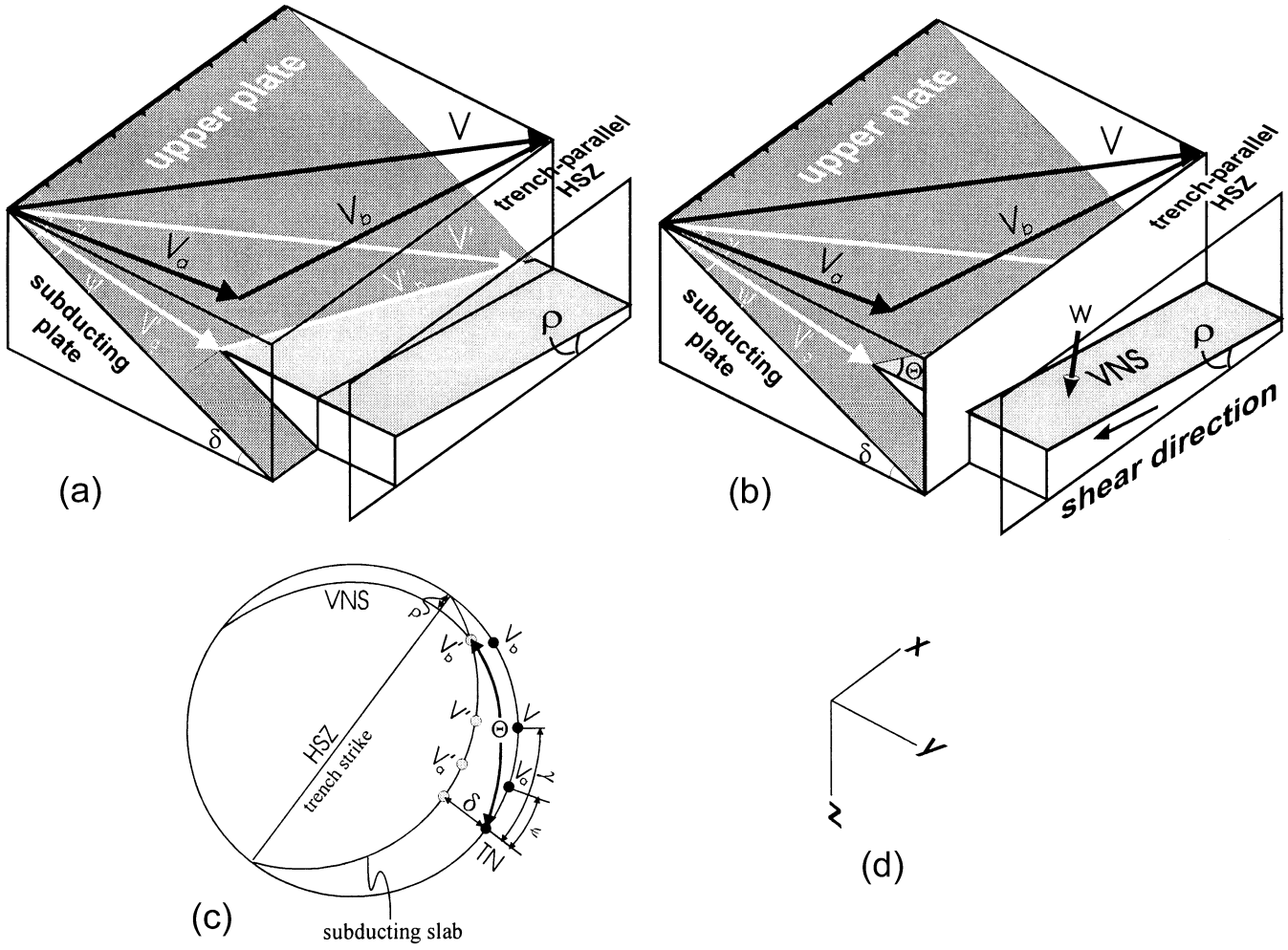

Fig. 9. Block diagram showing the three-dimensional geometry of general slip partitioning in a transpressional plate boundary. (a) The slip components of the subducting plate before entering the subduction zone are **v,** $\mathbf{v}_a$ and $\mathbf{v}_b$; after entering the zone they become $\mathbf{v}'$, $\mathbf{v}'_a$, and $\mathbf{v}'_b$, which are rigidly-rotated versions of **v**, $\mathbf{v}_a$ and $\mathbf{v}_b$. (b) The resolved shear direction on a vertical trench-parallel high-strain zone has a plunge of ρ leading to triclinic deformation. **W** is the vorticity vector and VNS stands for vorticity-normal section. (c) The geometrical relationship presented on an equal-area net between velocity components, subducting slab dip δ, partitioning of the obliquity of net slip, Θ angle and the resulting shear direction ρ. (d) The coordinate system used.

$\kappa = 0$ and $\kappa = 1$ are two end member cases of no obliquity partitioning and complete obliquity partitioning of Fitch (1972). McCaffrey's model deals with all of the intermediate cases of $0 \leq \kappa \leq 1$. In Sumatra for example, $\kappa \approx 0.56$ using the data of Molnar (1992).

In both the models of Fitch (1972) and McCaffrey (1992), only the partitioning of the *direction* of slip (obliquity) is considered. They implicitly assume that *all* of the convergence component of the net slip is accommodated by subduction slip (i.e., $v \cos \gamma = v_a \cos \psi$) and therefore the trench-parallel high-strain zone in the arc accommodates pure strike-slip motion. This is the same as assuming that $\mathbf{v}_b$ is always exactly parallel to the trench. But there is abundant evidence that trench-normal shortening is also accommodated by forearc deformation. We think that this trench-normal shortening component is too important to be ignored. A complete characterization of slip partitioning in a transpressional plate boundary region should therefore include also the partitioning of the convergence component of the net slip. This leads to our general partitioning scheme shown in Fig. 8c. Similar to Liu et al. (1995), we define a parameter ζ to measure the degree of convergence component partitioning:

$$\zeta = 1 - v_a \cos \psi / (v \cos \gamma). \quad (3)$$

$\zeta = 0$ for situations covered by the models of Fitch (1972) and McCaffrey (1992), where all of the convergence component is taken up by subduction slip. Generally, $0 < \zeta \leq 1$ and there is convergence component partitioning.

3.2. Bulk deformation path in trench-parallel high-strain zones

The following analysis assumes that all forearc deformation accommodating $\mathbf{v}_b$ is confined to a broad vertical

trench-parallel high-strain zone. We demonstrate that once there is convergence component partitioning ($0 < \zeta \leq 1$); the bulk deformation path in such a zone will be triclinic. In reality, deformation across a forearc is heterogeneously distributed (i.e., there are higher and lower strain zones within the broad zone, and they are variably oriented). To examine a specific zone in the forearc, one has to consider its immediate boundary condition, i.e., the further partitioning of $\mathbf{v}_b$ within the arc. For the purpose of this paper, it is sufficient to consider the broad zone, in order to draw the conclusion that deformation path in the forearc area is generally triclinic.

Fig. 9 is a block diagram showing the three-dimensional geometry of a general slip partitioning in a transpressional plate boundary. In the coordinate system xyz (same as in Fig. 7), the velocity components of the subducting plate before entering the subduction zone ($\mathbf{v}$, $\mathbf{v}_a$ and $\mathbf{v}_b$ in Fig. 9a) can be expressed as:

$$\mathbf{v} = v \sin \gamma \mathbf{i} + v \cos \gamma \mathbf{j}, \tag{4a}$$

$$\mathbf{v}_a = v_a \sin \psi \mathbf{i} + v_a \cos \psi \mathbf{j}, \text{ and} \tag{4b}$$

$$\mathbf{v}_b = \mathbf{v} - \mathbf{v}_a = (v \sin \gamma - v_a \sin \psi)\mathbf{i} + (v \cos \gamma - v_a \cos \psi)\mathbf{j}, \tag{4c}$$

where $\mathbf{i}$, $\mathbf{j}$, and $\mathbf{k}$ are unit vectors parallel to the *x*-, *y*-, and *z*-axes, respectively.

On the subduction interface, much like a conveyor belt, the magnitudes and the internal angular relationship among the three velocity components remain unchanged (Fig. 9c), but the subducting slab is now rotated downwards (Figs. 7 and 9). The three velocity components on the subduction interface, $\mathbf{v}'$, $\mathbf{v}'_a$, and $\mathbf{v}'_b$ (Fig. 9a) can be expressed in the coordinate system *xyz* as:

$$\mathbf{v}' = v \sin \gamma \mathbf{i} + v \cos \gamma \cos \delta \mathbf{j} + v \cos \gamma \sin \delta \mathbf{k} \tag{5a}$$

$$\mathbf{v}'_a = v_a \sin \psi \mathbf{i} + v_a \cos \psi \cos \delta \mathbf{j} + v_a \cos \psi \sin \delta \mathbf{k}, \text{ and} \tag{5b}$$

$$\mathbf{v}'_b = \mathbf{v}' - \mathbf{v}'_a = (v \sin \gamma - v_a \sin \psi)\mathbf{i} + (v \cos \gamma - v_a \cos \psi) \cos \delta \mathbf{j} + (v \cos \gamma - \mathbf{v}_a \cos \psi) \sin \delta \mathbf{k}, \tag{5c}$$

where δ is the angle of subduction. $\mathbf{v}'_a$ is accommodated by subduction slip whereas $\mathbf{v}'_b$ is accommodated by the trench-parallel high-strain zone deformation. $\mathbf{v}'_b$ is generally not parallel to the high-strain zone boundary; it makes an angle Θ with respect to the high-strain zone normal, and for a vertical high-strain zone, Θ is related to the slip components and subduction geometry by:

$$\Theta = \cos^{-1}\left(\frac{\mathbf{j}\cdot\mathbf{v}'_b}{|\mathbf{v}'_b|}\right) = \cos^{-1}\frac{(v \cos \gamma - v_a \cos \psi) \cos\delta}{\sqrt{v_a^2 + v^2 - 2vv_a \cos(\gamma - \psi)}}. \tag{6}$$

Generally, $0 < \Theta < 90°$.

$\mathbf{v}'_b$ has a boundary-parallel component leading to a component of simple shear in the trench-parallel high-strain zone. The angle ρ between the shear direction and the strike of the high-strain zone can be related to the slip components and subduction geometry by:

$$\rho = \tan^{-1}\left(\frac{(v \cos \gamma - v_a \cos \psi) \sin \delta}{v \sin \gamma - v_a \sin \psi}\right). \tag{7}$$

Eqs. (6) and (7) are valid for vertical high-strain zones. If the trench-parallel high-strain zone is inclined, its Θ and ρ can still be related to the plate slip components and subduction geometry once the dip of the high-strain zone is known. Unless there is no convergence component partitioning ($\zeta = 0$) and therefore $\rho = 0°$, ρ is commonly between 0 and 90° for the trench-parallel high-strain zone. This implies that the deformation path in such zones will generally be triclinic, according to Jiang and Williams (1998a). The angle Θ is related to the ratio of simple shear to the pure shear component within the zone (see below) with $\Theta = 0°$ representing the end member of pure shear, $\Theta = 90°$ the end member of simple shear, and $0° < \Theta < 90°$ a combination of pure shear and simple shear (Jiang and Williams, 1998a). Both Θ and ρ from Eqs. (6) and (7) are an average value for the high-strain zone. Generally they are expected to vary along the strike of the trench because of variation in the plate net slip $\mathbf{v}$ and dip of subduction δ along the trench line, both leading to variation of $\mathbf{v}'_b$. In addition, both Θ and ρ are commonly heterogeneously distributed across a high-strain zone (Lin et al., 1998).

3.3. Trench-parallel strain rates

An order of magnitude estimate of the strain rate, $\dot{\epsilon}_s$, parallel to the strike of the trench-parallel high-strain zone can be made using the available data. The slip component to be taken up by deformation within a trench-parallel high-strain zone in the forearc has a horizontal component parallel to the trench, $\mathbf{v}_s$, of (the $\mathbf{i}$-component of Eq. (4c) or Eq. (5c))

$$v_s = v \sin \gamma - v_a \sin \psi. \tag{8}$$

This equation reduces to eq. (6) of McCaffrey (1992) when there is no convergence component partitioning ($\zeta = 0$).

If v_s varies along the trench, the forearc high-strain zone will be either stretched ($\dot{\epsilon}_s = dv_s/dx > 0$) or shortened

($\dot{\epsilon}_s = dv_s/dx < 0$). Differentiating (8) yields:

$$\epsilon_s = \frac{dv_s}{dx} = \frac{dv}{dx}\sin\gamma + v\cos\gamma\frac{d\gamma}{dx} - \frac{dv_a}{dx}\sin\psi - v_a\cos\psi\frac{d\psi}{dx}. \quad (9)$$

v, γ and ψ in Eq. (9) can be observed directly in an active plate boundary. Using the parameter ζ defined in Eq. (3), after a slightly tedious but otherwise straightforward derivation, Eq. (9) can be rewritten as:

$$\frac{dv_s}{dx} = \frac{dv}{dx}\sin\gamma + v\frac{d\gamma}{dx}[\cos\gamma + (1-\zeta)\sin\gamma\tan\psi] + v\cos\gamma\tan\psi\frac{d\zeta}{dx} - v\cos\gamma(1-\zeta)\sec^2\psi\frac{d\psi}{dx}. \quad (10)$$

McCaffrey (1992) analyzed the force balance in the forearc plate boundary and showed that, because the shear stress supported by the trench-parallel high-strain zone is limited by the rock strength, the angle ψ will reach a maximum, ψ_{max}, while γ can have any value greater than ψ_{max}. Following this line of argument, ψ in a trench is dependent on the rheology, not the geometry, of the arc. It is therefore reasonable to further assume that in a natural subduction zone $\psi = \psi_{max}$ and $d\psi/dx = 0$. This reduces Eq. (10) to:

$$\frac{dv_s}{dx} = \frac{dv}{dx}\sin\gamma + v\frac{d\gamma}{dx}[\cos\gamma + (1-\zeta)v\sin\gamma\tan\psi_{max}] + v\cos\gamma\tan\psi_{max}\frac{d\zeta}{dx}. \quad (11)$$

While the obliquity partitioning of a trench can be directly observed, the partitioning of the convergence component (ζ) is very difficult to quantify. However, a trench may be divided into segments, within each of which the convergence component partitioning is approximately constant. In such a segment, the third term on the right side of Eq. (11) vanishes and Eq. (11) becomes:

$$\frac{dv_s}{dx} = \frac{dv}{dx}\sin\gamma + v\frac{d\gamma}{dx}[\cos\gamma + (1-\zeta)v\sin\gamma\tan\psi_{max}]. \quad (12)$$

Using the data set of McCaffrey (1992) for Sumatra: $\psi_{max} = 20 \pm 5°$, $d\gamma/dx = 0.0207 \pm 0.0031$ deg/km (change in obliquity of 58° along 2800 km length of the trench between 6°N, 92°E and 10°S, 110°E), and v is constant ($dv/dx = 0$) at 70 mm/year. These numbers with their uncertainties, together with $0 < \zeta < 1$, predict that $\dot{\epsilon}_s$ is $1.7–3.1 \times 10^{-8}$/year (or $5.4–9.8 \times 10^{-16}$/s) for southwest of southern Sumatra where $\gamma = 40°$, and $0.7–2.3 \times 10^{-8}$/year (or $2.2 \sim 7.3 \times 10^{-16}$/s) for southwest of northern Sumatra where $\gamma = 70°$. Similar estimates for Phillippine Trench and Aleutians yield results of the same order of

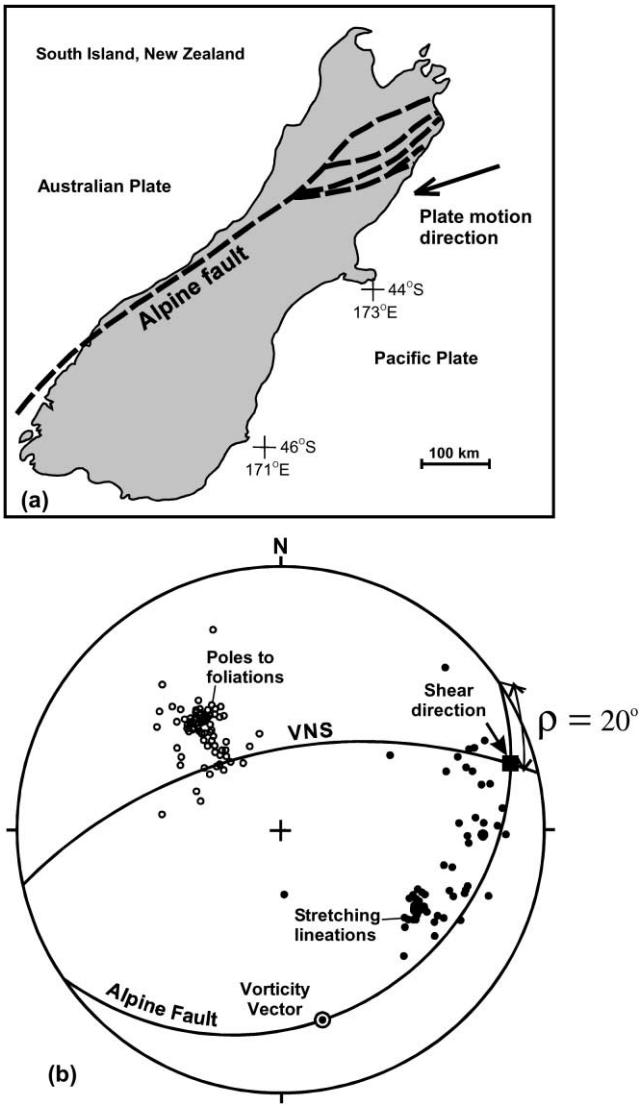

Fig. 10. (a) Map of South Island, New Zealand, showing the general geometry of the Alpine fault (modified from Teyssier et al., 1995). The plate motion direction (073°) is based on Walcott (1998). (b) Equal-area lower-hemisphere projection showing the structural geometry of the central segment of the Alpine fault. The foliation and lineation data are compiled from Sibson et al. (1979, Fig. 6a–e). The strike of the fault is 055° (well defined) and the dip of the fault is shown as 30° based on Norris and Cooper (1997), although its exact value is unknown. The shear direction is shown as being parallel to the plate motion direction because there is no discernable obliquity partitioning (Norris and Cooper 1997 and references therein). The general geometry is clearly triclinic; the lineations do not plot on the vorticity-normal section (VNS), but vary between the VNS and the dip line of the fault. Note that this conclusion will not be affected by possible variation in the dip of the fault. Movement along the fault is dextral reverse. Sibson et al. (1979) demonstrate that the average foliation has a more northerly strike than the fault (by ~6°) because of the dextral component of the movement. It is therefore reasonable to expect that the fault has a shallower dip than the average foliation because of the reverse component of the movement. In any case, the fault should not be steeper than the average foliation. A seismic survey across the central Alps indicates a structure dipping of 40–50° SE down to 20–30 km at least (Daveys et al., 1998). However, it is not known whether the structure imaged is the foliation or the fault zone boundary.

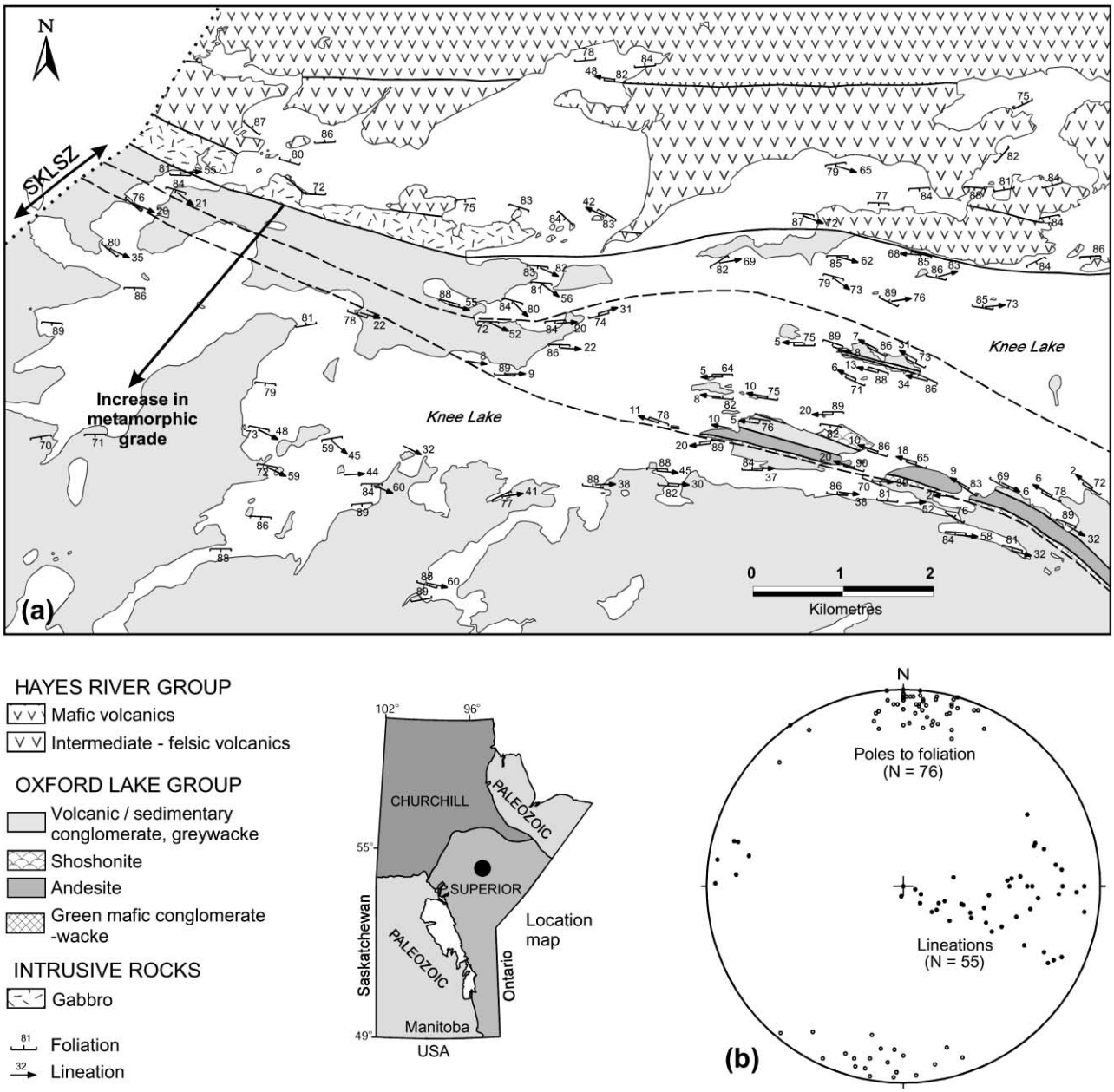

Fig. 11. (a) Simplified geological map of the southern Knee Lake area in the Oxford Lake–Knee Lake greenstone belt of the Superior Province of Manitoba, Canada. SKLSZ: Southern Knee Lake shear zone. Note that the lineation plunges shallowly near the center of the shear zone (approximately between the two long, thin dashed lines) and progressively steepens towards both margins. (b) Equal-area lower-hemisphere projection of foliation and lineation data for the shear zone. Great circle represents the overall shear zone orientation. See text for discussion.

magnitude (cf. McCaffrey, 1992). Although compared with the shear strain rate in a typical shear zone, which can be as high as 10^{-10}/s (Sibson, 1977; White and Mawer, 1992), the strike-length change at a rate of the order of 10^{-15}/s appears a minor phenomenon, but the accumulated strike-length stretch on the geological time scale can be significant. At a rate of 10^{-15}/s, the stretches along the strike are, respectively, 117%, 137% and 188% after 5, 10 and 20 million years.

4. Natural examples of triclinic high-strain zones

Lin et al. (1998) report a natural example of shear zones with strain geometry resembling the triclinic cases in Fig. 6, the Roper Lake shear zone in the Canadian Appalachians. We report here on two other examples of such shear zones. One is the currently active Alpine Fault in New Zealand and the other is the Southern Knee Lake shear zone in the Superior Province of the Canadian Shield.

4.1. The Alpine Fault: a currently active triclinic thinning zone

The Alpine Fault separates the Australian Plate from the Pacific Plate in South Island, New Zealand (Fig. 10a). The fault has a documented total dextral strike-slip displacement of 480 km (Wellman, 1955). Prior to 6.4 Ma, relative plate motion was strike-slip with only a small compressive component; since 6.4 Ma, the boundary has become transpressional and some 90 km of shortening has occurred in the continental crust of central South Island, together with 230 km of dextral strike-slip (Walcott, 1979, 1998; Allis, 1986; Kamp et al., 1989).

Compression has led to crustal thickening, in the form of the Southern Alps and their root. The Alps have been lowered by erosion (Walcott, 1998) resulting in the exhumation of amphibolite-facies rocks from depths of 20–25 km (Wellman, 1979; Cooper, 1980).

The central segment of the Alpine Fault appears to be very straight, striking 055°, and is sharply defined on regional maps (Cooper and Norris, 1994; Norris and Cooper, 1995; Walcott, 1998) although at shallow level the geometry is more complex in detail (Norris et al. 1990; Norris and Cooper, 1995). The vector describing the relative plate motion in the central segment of the fault near Franz Josef trends 073° (Walcott, 1998) or in other words is inclined at 15–20° to the average strike of the Alpine fault within South Island (Norris and Cooper, 1997).

A number of authors have pointed out that the central section of the Alpine Fault shows little discernable obliquity partitioning (Norris et al., 1990; Norris and Cooper, 1997 and references therein), but the compression (convergence component) is partitioned over a wide zone of at least 100 km width (Walcott, 1978) and almost double this in Otago (Norris et al., 1990). The most intense crustal thickening and erosion occur near the fault zone (Norris et al., 1990; Walcott, 1998). Walcott (1998) argued that a 5-km-thick tabular body of high-grade schist near the middle of the Alpine Fault is being extruded from the lower crust.

As the resolved shear direction on the Alpine Fault is not parallel to the strike of the fault nor parallel to the dip ($\rho \approx 20°$, Fig. 10b), and because the fault accommodates part of the compression, we expect the resultant deformation path within the fault zone to be triclinic. This is indeed supported by the foliation and stretching lineation data of Sibson et al. (1979) (Fig. 10b). The stretching lineations and poles to foliations do not plot on the VNS of the fault as would be the case if the deformation path had been monoclinic. Instead the lineations vary in pitch between the VNS and the dip line of the fault and the maxima of poles to foliations plot slightly above the VNS. Comparing Fig. 6 with Fig. 10b suggests that the Alpine Fault is a dip-lengthening-dominant dextral reverse triclinic thinning zone (case 1 of Fig. 6b). The ad hoc explanation that the variation in the direction of stretching lineations along the Alpine fault indicates a variation in the movement direction (Walcott, 1998) is unnecessary. It is more likely that the movement direction is nearly constant and the spread of lineations reflects variation in the amount of finite strain and/or variation in the ratio of the simple shear to the pure shear component, as predicted by triclinic high-strain zone models (Figs. 5 and 6).

4.2. Southern Knee Lake shear zone

The Southern Knee Lake shear zone is located in the Oxford Lake–Knee Lake greenstone belt of the Archean Superior Province of Manitoba, Canada (Fig. 11a). Supracrustal rocks in the belt consist of two stratigraphic groups (Fig. 11a): the older Hayes River Group (ca. 2830 Ma), composed of pillowed basalt and minor intermediate to felsic volcanic rocks and volcanogenic sedimentary rocks, and the younger Oxford Lake Group (ca. 2706 Ma), consisting of conglomerate, sandstone and minor andesite and shoshonite lavas (Syme et al. 1997 and references therein). Regionally, the Oxford Lake Group unconformably overlies the Hayes River Group. In the study area, the contact between the two groups is sheared and approximately coincides with the northern margin of the Southern Knee Lake shear zone. Rocks in the area are variably metamorphosed with metamorphic grade increasing from greenschist facies in the north to amphibolite facies in the south (Fig. 11a).

The Southern Knee Lake shear zone mainly affects the Oxford Lake Group (Fig. 11a) and the following description is based on observations made within the group. The shear zone strikes east-southeast in the study area. In the shear zone, both foliation and lineation are well developed. The foliation is defined by transposed bedding, mineral alignment and flattened clasts in fragmental rocks. It dips steeply everywhere (Fig. 11a and b). The lineation is defined by the long axis of elongated clasts and preferred orientation of elongate minerals (such as amphibole). It varies in orientation (Fig. 11a and b), from subhorizontal to down dip. Near the centre of the shear zone, the lineation is subhorizontal. Towards the margins on both sides, the lineation steepens progressively. The variation is gradual, and detailed mapping shows that the fabric is a product of a single generation of deformation. Field estimates based on shapes of deformed clasts in fragmental rocks suggest that the deformation is of flattening type ($0 < K < 1$). Kinematic indicators are best developed on subhorizontal surfaces, irrespective of the orientation of the lineation. They all indicate dextral shearing. The lineation orientations and the southward increase in metamorphic grade indicate that the zone boundary-parallel shearing also has a small south-over-north dip slip component. The simplest interpretation of this structural association indicates that the shear zone is a dextral oblique transpressional zone with triclinic symmetry as clearly shown in Fig. 11b.

5. Conclusions

Deformation paths in natural high-strain zones are expected to be generally triclinic and monoclinic paths are special end members. Fabrics observed in natural shear zones and theoretical arguments from continuum mechanics are compatible with this conclusion. Progress in our understanding of the kinematics of high-strain zones helps us interpret the structural geometries observed in natural shear zones. It is also a first and essential step in future attempts to analyze non-steady deformation paths by means of a realistic mechanic approach.

The relative convergence vector between the two boundaries of a high-strain zone is parallel to a flow appophysis *only for* a constant strike-length constant volume monoclinic transpression (Sanderson and Marchini) zone.

Complete characterization of slip partitioning in a transpressional plate boundary region requires not only obliquity partitioning but also partitioning of the convergence component. In the event that the convergence component is partitioned, the bulk deformation path in a trench-parallel high-strain zone within the arc is triclinic. Because the partitioning of the convergence component is likely to be common in transpressional plate boundary regions, the bulk deformation paths in these regions are generally expected to be triclinic.

Strike-length-constant transpression is a special case. Generally, the forearc area can be stretched or shortened along the strike of the trench. Estimates of currently active subduction zones show that the rates of stretch are on the order of 10^{-15}/s.

The Alpine Fault in the South Island of New Zealand and the Southern Knee Lake shear zone of Manitoba, Canada provide active and Archean examples, respectively, of triclinic shear zones.

Acknowledgements

The field work on the Southern Knee Lake shear zone was conducted when SL was employed by Manitoba Energy and Mines (now Manitoba Industry, Trade and Mines); DJ thanks Ric Syme and Tim Corkery for involving him in the project and for logistic support. PFW acknowledges support from an NSERC research grant. We thank Drs R.J. Norris and R.H. Sibson for providing information on the Alpine Fault, Win Means and Wouter Bleeker for review comments, and Tim Little for discussion. The paper was presented at the 1998 GAC NUNA conference held in Canmore, Alberta. Feedback from and discussion with the audience is appreciated.

References

Abers, G., McCaffrey, R., 1988. Active deformation in the New Guinea fold-and-thrust belt: seismological evidence for strike-slip faulting and basement-involved thrusting. Journal of Geophysical Research 93, 13 332–13 534.

Allis, R.G., 1986. Mode of crustal shortening adjacent to the Alpine fault, New Zealand. Tectonics 5, 15–32.

Astarita, G., 1979. Objective and generally applicable criteria for flow classification. Journal of Non-Newtonian Fluid Mechanics 6, 69–76.

Beck, M., 1983. On the mechanism of tectonic transport in zones of oblique subduction. Tectonophysics 93, 1–11.

Bodyarchik, A.R., 1986. The eigenvalues of steady flow in Mohr space. Tectonophysics 122, 35–51.

Brown, M., Solar, G.S., 1998a. Shear zones and melts: positive feedback in orogenic belts. Journal of Structural Geology 20, 211–227.

Brown, M., Solar, G.S., 1998b. Granite ascent and emplacement during contractional deformation in convergent orogens. Journal of Structural Geology 20, 1365–1393.

Carter, N.L., Kirby, S.H., 1978. Transient creep and semibrittle behavior of crystalline rocks. Pure and Applied Geophysics 116, 807–839.

Carter, N.L., Tsenn, M.C., 1987. Flow properties of continental lithosphere. Tectonophysics 136, 27–63.

Cooper, A.F., 1980. Retrograde alteration of chromium kyanite in metachert and amphibolite whiteschist from the Southern Alps, New Zealand, with implications for uplift on the Alpine Fault. Contributions to Mineralogy and Petrology 75, 153–164.

Cooper, A.F., Norris, R.J., 1994. Anatomy, structural evolution, and slip rate of a plate-boundary thrust: the Alpine fault at Gaunt Creek, Westland, New Zealand. Geological Society of America Bulletin 106, 627–633.

Daveys, F.J., Henyey, T., Holbrook, W.S., Okaya, D., Stern, T.A., et al., 1998. Preliminary results from a geophysical study across a modern, continent-continent collisional plate boundary—the Southern Alps, New Zealand. Tectonophysics 288, 221–235.

DeMets, C., Gordon, R.G., Argus, D.F., Stein, S., 1990. Current plate motions. Geophys. Journal Int. 101, 425–478.

Dewey, J.F., 1980. Episodicity, sequence, and style at convergent plate boundaries. The Continental Crust and Its Mineral Deposits, Strangway, D.W. (Ed.). Geological Association of Canada Special Paper 20, 553–573.

Dewey, J.F., Holdsworth, R.E., Strachan, R.A., 1998. Transpression and transtension zones. Continental Transpressional and Transtensional Tectonics, Holdsworth, R.E., Strachan, R., Dewey, J.F. (Eds.). Geological Society Special Publication 135, 1–14.

Dutton, B.J., 1997. Finite strains in transpression zones with no boundary slip. Journal of Structural Geology 19, 1189–1200.

England, P.C., Jackson, J., 1989. Active deformation of the continents. Annual Review of Earth and Planetary Sciences 17, 197–226.

England, P.C., Houseman, G.A., Sonder, L.J., 1985. Length scales for continental deformation in convergent, divergent, and strike-slip environments: analytical and approximate solutions for a thin viscous sheet model. Journal of Geophysical Research 90, 3551–3557.

Fitch, T.J., 1972. Plate convergence, transcurrent faults, and internal deformation adjacent to Southeast Asia and the western Pacific. Journal of Geophysical Research 77, 4432–4460.

Fletcher, R.C., Pollard, D.D., 1999. Can we understand structural and tectonic processes and their products without appeal to a complete mechanics? Journal of Structural Geology 21, 1071–1088.

Fossen, H., Tikoff, B., 1993. The deformation matrix for simultaneous simple shearing, pure shearing and volume change, and its application to transpression–transtension tectonics. Journal of Structural Geology 15, 413–422.

Fossen, H., Tikoff, H., 1997. Forward modeling of non-steady-state deformations and the 'minimum strain path'. Journal of Structural Geology 19, 987–996.

Fossen, H., Tikoff, B., 1998. Extended models of transpression and transtension, and application to tectonic settings. Continental Transpressional and Transtensional Tectonics, Holdsworth, R.E., Strachan,

R., Dewey, J. (Eds.). Geological Society Special Publication 135, 15–33.

Fossen, H., Tikoff, B., Teyssier, C., 1994. Strain modeling of transpressional and transtensional deformation. Norsk Geologish Tidsskrift 74, 134–145.

Goodwin, L.B., Williams, P.F., 1996. Deformation path partitioning within a transpressive shear zone, Marble Cove, Newfoundland. Journal of Structural Geology 18, 975–990.

Gordon, R.G., 1995. Plate motions, crustal and lithospheric mobility, and paleomagnetism: prospective viewpoint. Journal of Geophysical Research 100, 24367–24392.

Harland, W.B., 1971. Tectonic transpression in Caledonian Spitsbergen. Geological Magazine 108, 27–42.

Hobbs, B.E., Ord, A., 1988. Plastic in stability: implications for the origin of intermediate and deep focus earthquakes. Journal of Geophysical Research 93, 10521–10540.

Hudleston, P.J., Schultz-Ela, D., Southwick, D.L., 1988. Transpression in an Archean greenstone belt, northern Minnesota. Canadian Journal of Earth Sciences 25, 1060–1068.

Jarrard, R.D., 1986. Terrane motion by strike-slip faulting of forearc slivers. Geology 14, 780–783.

Jiang, D., 1994a. Vorticity determination, distribution, partitioning and the heterogeneity and non-steadiness of natural deformations. Journal of Structural Geology 16, 121–130.

Jiang, D., 1994b. Flow variation in layered rocks subjected to bulk flow of various kinematic vorticities: theory and geological implications. Journal of Structural Geology 16, 1159–1172.

Jiang, D., 1998. Forward modeling of non-steady-state deformations and the 'minimum strain path': Discussion. Journal of Structural Geology 20, 975–977.

Jiang, D., 1999. Vorticity decomposition and its application to sectional flow characterization. Tectonophysics 301, 243–259.

Jiang, D., White, J.C., 1995. Kinematics of rock flow and the interpretation of geological structures, with particular reference to shear zones. Journal of Structural Geology 17, 1249–1265.

Jiang, D., Williams, P.F., 1998a. High-strain zones: a unified model. Journal of Structural Geology 20, 1105–1120.

Jiang, D., Williams, P.F., 1998b. Triclinic high-strain zones. GSA Abstract with Programs 30, A-133.

Jiang, D., Williams, P.F., 1999a. When do dragfolds not develop into sheath folds in shear zones? Journal of Structural Geology 21, 577–583.

Jiang, D., Williams, P.F., 1999b. A fundamental problem with the kinematic interpretation of geological structures. Journal of Structural Geology 21, 933–937.

Jones, R.R., Holdsworth, R.E., Baily, W., 1997. Lateral extrusion in transpression zones. Journal of Structural Geology 19, 1201–1217.

Kamp, P.J.J., Green, P.F., White, S.H., 1989. Fisson track analysis reveals character of collision tectonics in New Zealand. Tectonics 8, 169–195.

Kao, H., Shen, S., Ma, K.-F., 1998. Transition from oblique subduction to collision: Earthquakes in the southernmost Ryukyu arc-Taiwam region. Journal of Geophysical Research 103, 7211–7229.

Kohlstedt, D.L., Evans, B., Mackwell, S.J., 1995. Strength of the lithosphere: constraints imposed by laboratory experiments. Journal of Geophysical Research 100, 17 587–17 602.

Lin, S., 1992. The stratigraphy and structural geology of the southeastern Cape Breton Highlands National Park and its implications for the tectonic evolution of Cape Breton Island, Nova Scotia, with emphasis on lineations in shear zones, PhD thesis, University of New Brunswick.

Lin, S., Jiang, D., Williams, P.F., 1998. Transpression (or transtension) zones of triclinic symmetry: natural example and theoretical modeling. Continental Transpressional and Transtensional Tectonics, Holdsworth, R.E., Strachan, R., Dewey, J.F. (Eds.). Geological Society Special Publication 135, 41–57.

Lin, S., Jiang, D., Williams, P.F., 1999. Discussion on transpression and transtension zones. Journal of the Geological Society, London 156, 1045–1048.

Lister, G.S., Williams, P.F., 1983. The partitioning of deformation in flowing rock masses. Tectonophysics 92, 1–33.

Liu, X., McNally, K.C., Shen, Z.-K., 1995. Evidence for a role of the downgoing slab in earthquake slip partitioning at oblique subduction zones. Journal of Geophysical Research 100, 15351–15372.

McCaffrey, R., 1991. Slip vectors and stretching of the Sumatran forearc. Geology 19, 881–884.

McCaffrey, R., 1992. Oblique plate convergence, Slip vectors, and forearc deformation. Journal of Geophysical Research 97, 8905–8915.

McCaffrey, R., 1993. On the role of the upper plate in great subduction zone earthquakes. Journal of Geophysical Research 98, 11953–11966.

McCaffrey, R., 1994. Global variability in subduction thrust zone-forearc systems. Pure and Applied Geophysics 142, 173–224.

McKenzie, D., 1979. Finite deformation during fluid flow. Geophysical Journal of Royal Astronomy Society 58, 689–715.

McKenzie, D., Jackson, J., 1983. The relationship between strain rates, crustal thickening, paleomagnetism, finite strain and fault movements within a deformation zone. Earth and Planetary Science Letter 65, 182–202.

Means, W.D., 1995. Shear zones and rock history. Tectonophysics 247, 157–160.

Means, W.D., Hobbs, B.E., Lister, G.S., Williams, P.F., 1980. Vorticity and non-coaxiality in progressive deformations. Journal of Structural Geology 2, 371–378.

Micheal, A.J., 1990. Energy constraints on kinematic models of oblique faulting: Loma Prieta versus Parkfield-Coalinga. Geophysical Research Letters 17, 1453–1456.

Molnar, P., 1988. Continental tectonics in the aftermath of plate tectonics. Nature 335, 131–137.

Molnar, P., 1992. Brace-Goetze strength profiles, the partitioning of strike-slip and thrust faulting at zones of oblique convergence, and the stress-heat flow paradox of the San Andreas fault. In: Evans, B., Wong, T. (Eds.). Fault Mechanics and Transport Properties of Rocks. Academic Press, San Diego, pp. 435–459.

Mount, V.S., Suppe, J., 1987. State of stress near the San Andreas fault: implications for wrench tectonics. Geology 15, 1143–1146.

Norris, R.J., Cooper, A.F., 1995. Origin of small-scale segmentation and transpressional thrusting along the Alpine fault, New Zealand. Bulletin of the Geological Society of America 107, 231–240.

Norris, R.J., Cooper, A.F., 1997. Erosional control on the structural evolution of a transpressional thrust complex on the Alpine Fault, New Zealand. Journal of Structural Geology 19, 1323–1342.

Norris, R.J., Koons, P.O., Cooper, A.F., 1990. The obliquely-convergent plate boundary in the South Island of New Zealand: implications for ancient collision zones. Journal of Structural Geology 12, 715–725.

Passchier, C.W., 1997. The fabric attractor. Journal of Structural Geology 19, 113–127.

Passchier, C.W., 1998. Monoclinic model shear zones. Journal of Structural Geology 20, 1121–1137.

Poirier, J.P., 1980. Shear localization and shear instability in materials in the ductile field. Journal of Structural Geology 2, 135–142.

Ramberg, H., 1975a. Particle paths, displacement and progressive strain applicable to rocks. Tectonophysics 28, 1–37.

Ramberg, H., 1975b. Superposition of homogeneous strain and progressive deformation in rocks. Bulletin of Geological Institute, University of Uppasala, N.S. 6.

Ramsay, J.G., 1980. Shear zone geometry: a review. Journal of Structural Geology 2, 83–89.

Ramsay, J.G., Graham, R.H., 1970. Strain variation in shear belts. Canadian Journal of Earth Sciences 7, 786–813.

Robin, P.-Y.F., Cruden, A.R., 1994. Strain and vorticity patterns in ideally ductile transpressional zones. Journal of Structural Geology 16, 447–466.

Sanderson, D.J., Marchini, W.R.D., 1984. Transpression. Journal of Structural Geology 6, 449–458.

Sibson, R.H., 1977. Fault rocks and fault mechanisms. Journal of Geological Society, London 133, 191–213.

Sibson, R.H., White, S.H., Atkinson, B.K., 1979. Fault rock distribution and structure within the Alpine fault zone: a preliminary account. The Origin of the Southern Alps, Walcott, R.I., Cresswell, M.M. (Eds.). Royal Society of New Zealand Bulletin 18, 55–65.

Spencer, A.J.M., 1980. Continuum mechanics. Longman, London.

Syme, E.C., Corkery, M.T., Bailes, A.H., Lin, S., Cameron, H.D.M., Prouse, D. 1997. Geological investigations in the Knee Lake area, northwestern Superior Province. Manitoba Energy and Mines, Minerals Division, Report of Activities, pp. 37–46.

Teyssier, C.B., Tikoff, B., Markley, M., 1995. Oblique plate motion and continental tectonics. Geology 23, 447–450.

Tikoff, B., Fossen, H., 1993. Simultaneous pure and simple shear: the unifying deformation matrix. Tectonophysics 217, 267–283.

Tikoff, B., Fossen, H., 1999. Three-dimensional reference deformations and strain facies. Journal of Structural Geology 21, 1497–1521.

Tsenn, M.C., Carter, N.L., 1987. Upper limits of power law creep of rocks. Tectonophysics 136, 1–26.

Walcott, R.I., 1978. Present tectonics and late Cenozoic evolution of New Zealand. Geophysical Journal of the Royal Astronomical Society 52, 137–164.

Walcott, R.I., 1979. Plate motion and shear strain rates in the vicinity of the Southern Alps. In: Walcott, R.I., Cresswell, M.M. (Eds.). The Origin of the Southern Alps. Royal Society of New Zealand Bulletin, 18, pp. 5–12.

Walcott, R.I., 1998. Modes of oblique compression: late Cenozoic tectonics of the South Island of New Zealand. Reviews of Geophysics 36, 1–26.

Wellman, H.W., 1955. New Zealand Quaternary tectonics. Geologisches Rundschau 43, 248–257.

Wellman, H.W., 1979. An uplift map for the South Island of New Zealand and a model for uplift of the Southern Alps. The Origin of the Southern Alps, Walcott, R.I., Cresswell, M.M. (Eds.). Royal Society of New Zealand Bulletin 18, 13–20.

White, J.C., Mawer, C.K., 1992. Deep-crustal deformation textures along megathrusts from Newfoundland and Ontario: implications for microstructural preservation, strain rates, and strength of the lithosphere. Canadian Journal of Earth Sciences 29, 328–337.